VOL. 11, NO. 24, DECEMBER 2016 ISSN 1819-6608
ARPN Journal of Engineering and Applied Sciences

www.arpnjournals.com

SHOCK WAVE INSTABILITY IN FRONT OF A CYLINDER OVER AN EXPANSION CORNER

Alexander Kuzmin
Department of Fluid Dynamics, St. Petersburg State University, Russia
E-Mail: a.kuzmin@spbu.ru

ABSTRACT

We study numerically transonic flow past a cylinder located above a convex corner. The cylinder produces a detached shock which interacts with the expansion flow region over the corner. Solutions of the Reynolds-averaged Navier-Stokes equations are obtained with a finite-volume solver of second-order accuracy on fine meshes. The dependence of 2D shock position on the free-stream Mach number, Reynolds number, corner angle, and rounding arc is studied. Also 3D flow simulations for two spans of the cylinder are discussed.

Keywords: shock wave, expansion flow, **i**nteraction, instability.

1. INTRODUCTION

In the last two decades, numerical simulations of inviscid and turbulent transonic flow demonstrated instability of double supersonic regions on airfoils comprising a flat segment or nearly flat arc [1- 4]. The instability arises due to an interaction between (i) the shock wave terminating the bow supersonic region and (ii) the front (sonic line) of the aft supersonic region.

The same type of instability occurs in channels with a bend or break of walls and a supersonic velocity at the inlet [5]. In this case, the shock wave forms in front of a compression ramp of a wall, whereas the sonic surface arises over the expansion corner of the opposite wall. A dependence of the shock location on the velocity profile given at the inlet was studied in [5, 6].

Instability of a detached shock wave, which forms ahead of a channel, was examined in [7]. The shock leg interaction with an expansion flow created at the channel throat was analyzed. Effects of the angle of attack on the shock behavior in the entrance region were studied. In practice, such a problem occurs, e.g., when a supersonic intake encounters variations of the incoming flow parameters because of the atmospheric turbulence or a maneuvering flight of aircraft [8, 9].

In [10] we explored the instability of a detached shock in front of a cylinder placed above an expansion corner. Free-stream Mach numbers M_∞ and streamwise coordinates x_c of the corner, at which the shock position is extremely sensitive to small perturbations, were determined for two radii of the cylinder.

This paper aims at further study of the problem examined in [10]. First, in Section 2 we formulate boundary conditions and outline a numerical method. Then in Section 3 we discuss 2D shock wave positions and their dependence on the corner angle θ, Mach number M_∞, Reynolds number, and a circular arc that rounds the corner. Section 4 addresses 3D flow simulations for two cylinders of finite span.

2. FORMULATION OF THE PROBLEM AND A NUMERICAL METHOD

For 2D flow simulation, we consider a plane (x,y) and a circle of radius r_1=0.003 m whose center is located at a height h=0.3 m and has an abscissa of 0.21 m. The circle is a cross section of the 3D cylinder of infinite span. In what follows, the Cartesian coordinates (x,y,z) and radius r_1 are non-dimensionalized by h ; hence, the coordinates of the circle center are x=0.7 and y=1, see Figure-1.

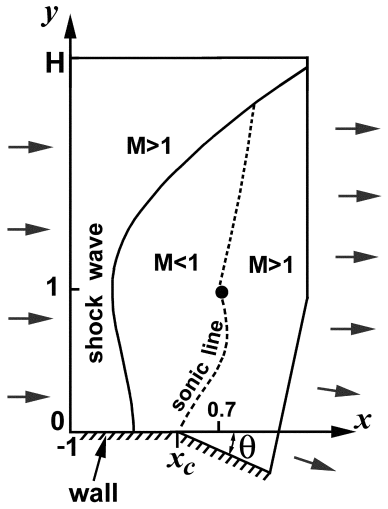

Figure-1. Sketch of the 2D computational domain and shock/sonic line location in the case θ>3.8°.

A wall with an expansion corner is given by the expressions

$$y=0 \text{ at } -1 \le x \le x_c, \quad y=-(x-x_c)\tan\theta \text{ at } x_c < x \le 1 \qquad (1)$$

where x_c=0.4.

The inlet boundary of the computational domain is set at x=−1, $0 \le y \le H$. The upper boundary $y=H$, $-1 \le x \le 1.5$ is remote at a distance H=16 from the wall in order to eliminate its influence on the flow between the wall and cylinder. The outlet boundary is constituted by a vertical segment x=1.5, $1 \le y \le H$, and a segment connecting the point x=1.5, y=1 with the end of wall x=1, $y=-(1-x_c)\tan\theta$.

The free stream is uniform and parallel to the x-axis. Therefore the x- and y-components of the flow velocity are

$U_\infty = M_\infty a_\infty$, $V_\infty = 0$, $W_\infty = 0$. (2)

At the inlet we prescribe the velocity components (2), static pressure $p_\infty = 10^5$ N/m^2, a turbulence level of 0.2%, and static temperature $T_\infty = 250$ K which determines the sound speed $a_\infty = 317.02$ m/s. At the outlet, a condition of the supersonic flow regime is imposed. On the wall (1) and cylinder we use the no-slip condition and vanishing heat flux. Initial data are either parameters of the uniform free stream or a flow field calculated for a different free-stream Mach number.

The air is treated as a perfect gas whose specific heat at constant pressure c_p is 1004.4 J/(kg K), the ratio $\gamma = c_p/c_v$ of specific heats is 1.4, and molar mass is 28.96 kg/kmol. The Sutherland formula is used for molecular dynamic viscosity.

The 2D turbulent flow is governed by the unsteady Reynolds-averaged Navier-Stokes equations with respect to velocity components $U(x,y,t)$, $V(x,y,t)$, density $\rho(x,y,t)$, and static temperature $T(x,y,t)$:

$$\rho_t + (\rho U)_x + (\rho V)_y = 0, \quad (3)$$

$$(\rho U)_t + (\rho U^2)_x + (\rho UV)_y = -p_x + \tau_x^{xx} + \tau_y^{xy}, \quad (4)$$

$$(\rho V)_t + (\rho UV)_x + (\rho V^2)_y = -p_y + \tau_x^{yx} + \tau_y^{yy}, \quad (5)$$

$$[\rho(c_v T + (U^2+V^2)/2)]_t + [\rho U(c_p T + (U^2+V^2)/2)]_x + [\rho V(c_p T + (U^2+V^2)/2)]_y =$$

$$= (kT_x + U\tau^{xx} + V\tau^{xy} + \sigma^x)_x + (kT_y + U\tau^{yx} + V\tau^{yy} + \sigma^y)_y, \quad (6)$$

where the subscripts t, x, y denote partial derivatives, and the static pressure p is related to ρ and T by the equation of state $p = \rho RT$, $R = c_p - c_v$. In (4)-(6), k is the thermal conductivity, whereas the vector (σ^x, σ^y) and tensor $(\tau^{xx}, \tau^{xy}, \tau^{yx}, \tau^{yy})$ govern flow viscosity and heat fluxes (see details in [11, p.232]). The local Mach number is $M = (U^2+V^2)^{1/2}/a$ where $a = (\gamma RT)^{1/2}$ is the sound speed.

Solutions of the system (3)-(6) were obtained with an ANSYS-15 CFX finite-volume solver of second-order accuracy, which is based on a high-resolution scheme for convective terms [12]. An implicit backward Euler scheme was employed for the time-accurate computations. We used a Shear Stress Transport k-ω turbulence model which is known to reasonably predict aerodynamic flows with boundary layer separations [13].

Numerical simulations of 2D flow were performed on hybrid meshes constituted by quadrangles in 39 layers on the wall and cylinder, and by triangles in the remaining region. The non-dimensional thickness y^+ of the first mesh layer on the wall and cylinder was less than 1. Apart from the boundary layer region, mesh nodes were clustered in vicinities of the expansion corner and shock waves. Test computations on uniformly refined meshes of approximately 10^5, 2×10^5, and 4×10^5 cells showed that a discrepancy between shock wave coordinates obtained on the second and third meshes did not exceed 1%. Global time steps of 10^{-6} s and 2×10^{-6} s yielded undistinguishable solutions. That is why we employed meshes of 2×10^5 cells and the time step of 2×10^{-6} s for the study of 2D transonic flow at various free-stream velocities. The root-mean-square CFL number (over mesh cells) was about 3. Simulations of 3D flow were performed in a domain that extends spanwise from $z=0$ to $z=4$, as described below in Section 4.

Free-stream Mach numbers under consideration lie in the range $1.075 \le M_\infty \le 1.1$. Therefore, the Reynolds number based on $h=0.3$ m is $Re \approx 7.9\times10^6$. In addition, a few computations were performed at $p_\infty = 2.3\times10^5$ N/m^2, $Re \approx 1.8\times10^7$ for comparison (Figure-5b).

The solver was verified by computation of several commonly used test cases, such as transonic flow over ONERA M6 wing [14] and flow in a channel with a circular-arc bump [6]. Also we performed computations of a shock in front of a circular cylinder of radius $r_2 = 0.006$ m in the absence of solid walls. At $M_\infty = 1.35$, the obtained distance d between the center of cylinder and shock was $6.32r_2$ for inviscid flow and $6.34r_2$ for turbulent flow ($Re = 3.9\times10^5$). This result matches perfectly experimental data documented in [15]. At M∞=1.6, the solver produced d=3.46r2 for inviscid flow and d=3.47r2 for turbulent flow; this is in a reasonable agreement with the value of 3.67r2

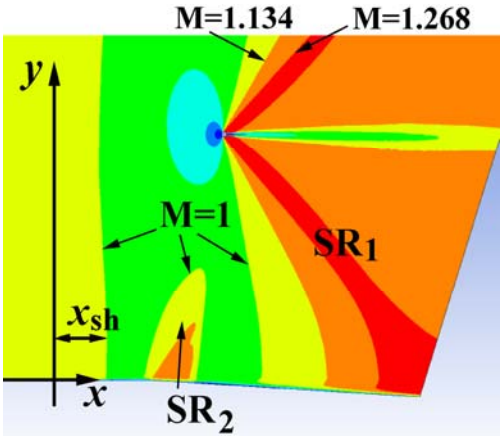

Figure-2. Mach number contours in the flow over wall (1).

at $M_\infty = 1.089$, $\theta = 3.5°$

obtained in experiments by Holder and Chinnek [16]. Calculated isoMachlines over the cylinder at $M_\infty = 1.1$ and $M_\infty = 1.3$ virtually coincided with ones computed by Bashkin *et al.* [17] (except for minor discrepancies in the near wake).

3. RESULTS OF 2D FLOW SIMULATIONS

Numerical simulations demonstrated a convergence of the solutions to steady states in less than 0.2 s of physical time. At $M_\infty < 1.1$, the obtained flow fields exhibit a large subsonic region between the detached shock and the sonic line emanating from the cylinder (see Figure-2). The sonic line is a front of the supersonic region SR_1 located downstream. If the expansion angle θ is less than

approximately 3.8°, then there exists another supersonic region SR_2 at the corner of the wall. The region SR_2 expands and gets into coalescence with SR_1 when θ increases and exceeds 3.8°.

To trace the streamwise position of the shock, we use the x-coordinate x_{sh} of its intersection with the horizontal line y=0.17 located above the boundary layer which forms on the wall. Computations showed that the shock coordinate x_{sh} as a function of the angle θ depends crucially on the Mach number M_∞. If $M_\infty \le 1.09$, then x_{sh} is proportional to the angle θ when $0 \le \theta \le 3°$ (curves 1-4 in Figure-3), whereas it is almost fixed when $5° \le \theta \le 16°$. The discontinuities of curves 2-4 are caused by jumps of the shock from a nearly vertical position ahead of the expansion corner to an oblique position in which its foot reaches a vicinity of the corner.

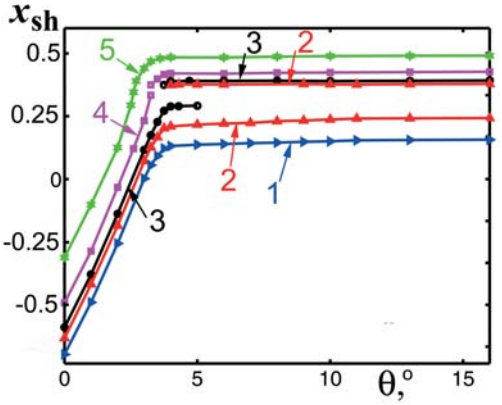

Figure-3. Dependence of the shock position x_{sh} on the expansion angle θ at various M_∞: 1 - 1.079, 2-1.082, 3 - 1.084, 4 - 1.089, 5 - 1.099.

Surfaces in Figure-4 illustrate x_{sh} as a function of two parameters, θ and M_∞, for turbulent and inviscid flows. As seen from Figure-4b, the qualitative behavior of the shock in inviscid flow is the same as in turbulent one, though the surface $x_{sh}(\theta, M_\infty)$ is shifted to smaller Mach numbers and angles θ. There is a narrow region in the plane (θ, M_∞) that admits a flow hysteresis.

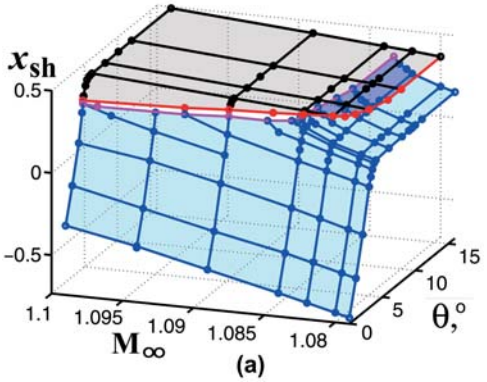

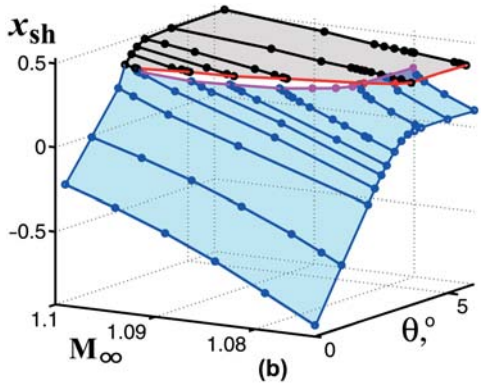

Figure-4. Shock wave coordinate x_{sh} as a function of M_∞ and expansion corner angle θ: (a) - 2D fully turbulent flow, (b) - 2D inviscid flow in a range $0 \le \theta \le 6°$.

Also flow simulations were performed for the wall with a rounded corner.

$$y = 0 \quad \text{at} \quad -1 \le x \le x_{c1}\,, \tag{7a}$$

$$y = -R + [\,R^2 - (x - x_{c1})\,]^{1/2} \quad \text{at} \quad x_{c1} < x < x_{c2}\,, \tag{7b}$$

$$y = -(x - x_c)\tan 5^\circ \quad \text{at} \quad x_{c2} \le x \le x_{out}\,. \tag{7c}$$

The circular arc (7b) is tangent to the segments (7a), (7c) at $x=x_{c1}$ and $x=x_{c2}$, respectively. Coordinates x_{c1} and x_{c2} for two values of R are given in Table-1. When $R \to 0$, one obtains $x_{c1} \to 0.4$, $x_{c2} \to 0.4$, that is the wall (1).

The insertion of arc (7b) produces a shift of the sonic line upstream to the beginning of the arc. Therefore the spacing between the shock and sonic line decreases, and their interaction develops at smaller free-stream Mach numbers.

Table-1. Parameters of the circular arc (7b): radius R and coordinates of endpoints.

R	x_{c1}	y_{c1}	x_{c2}	y_{c2}
0.5	0.37817	0	0.42167	−0.00190
1	0.35634	0	0.44334	−0.00379

Figure-5 demonstrates that, indeed, at R=0.5 and R=1 the jumps of x_{sh} are shifted to smaller values of M_∞, while the width of the hysteresis remains almost the same. An increase of the Reynolds number from 7.9×10^6 to 1.8×10^7 produces only a minor effect on the shock wave position; see the dashed curves in Figure-5.

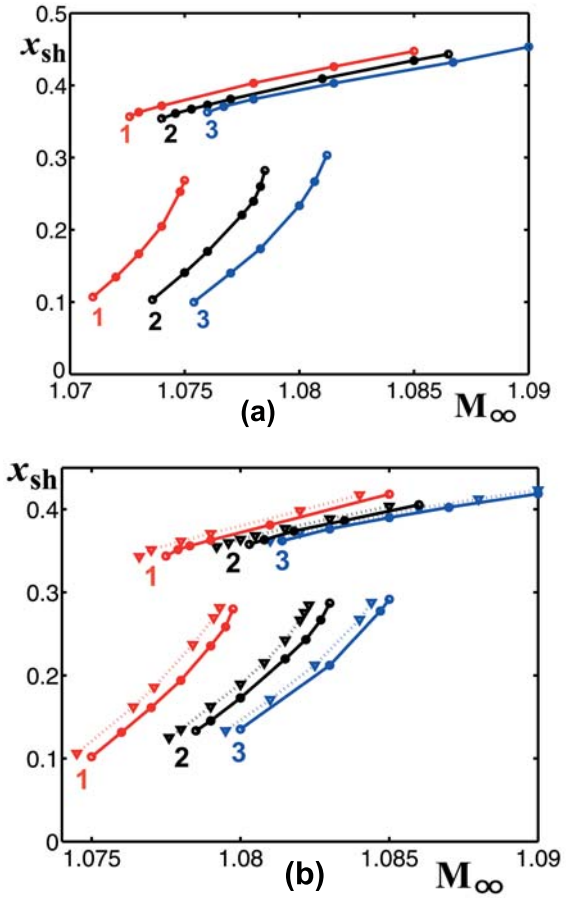

Figure-5. Shock wave position x_{sh} in transonic flow over walls (7) and (1): 1 - R=1, 2 – R=0.5, 3 - R=0; (a) inviscid flow, (b) turbulent flow: solid curves - Re=7.9×10^6, dashed curves - Re=1.8×10^7.

4. 3D FLOW SIMULATIONS

The outer boundary of the 3D computational domain was obtained by an extrusion of the 2D boundary (Figure. 2) from z=0 to z=4. The cylinder was created by an extrusion of the circle $(x-0.7)^2+(y-1)^2=10^{-4}$ from z=0 to z=L where L=1 or L=5/3.

On the plane z=0 we imposed a symmetry condition. On the side and top boundaries of the domain, a free-slip condition was used. A hybrid mesh was constituted by 9.5×10^6 prisms in 39 layers on the wall and cylinder, and by 15×10^6 tetrahedrons in the remaining region. Solutions of 3D Reynolds-averaged Navier-Stokes equations with respect to U, V, W, ρ, T were obtained with the method outlined in Section 2.

A comparison of the calculated Mach number contours in the plane z=0 shows that, for the span L=1, the subsonic region is noticeably smaller than the one in 2D flow. With increasing L from 1 to 5/3, the subsonic region enlarges, and the discrepancy decreases. Figure-6 shows the shock wave, 3D sonic surfaces, and Mach number contours in the plane z=0 for L=5/3, M_∞=1.1.

Since the upward and downward extensions of the 3D subsonic region for L=5/3 are yet smaller than those in 2D flow, one needs a smaller free-stream Mach number for an expansion of the region down to the wall. Computations revealed that this occurs at M_∞=1.056 (instead of 1.080 in 2D flow, see Figure-4a). Then the shock wave jumps to a position which is normal to the wall at a point upstream of the corner (Figure-7).

We notice that a replacement of the symmetry condition on the plane z=0 by the no-slip one produced a negligible effect on the shock and sonic surface positions.

5. CONCLUSIONS

Numerical solutions of the Reynolds averaged Navier-Stokes equations demonstrated that, if the expansion corner angle exceeds 3.5°, then there exist adverse free-stream Mach numbers admitting abrupt changes of the 2D shock position at small perturbations. This phenomenon is true for both turbulent and inviscid flows. If the expansion corner is rounded with a circular arc, the jumps of shock occur at smaller free-stream Mach numbers. The 3D flow computations have confirmed the shock wave instability at adverse free-stream Mach numbers.

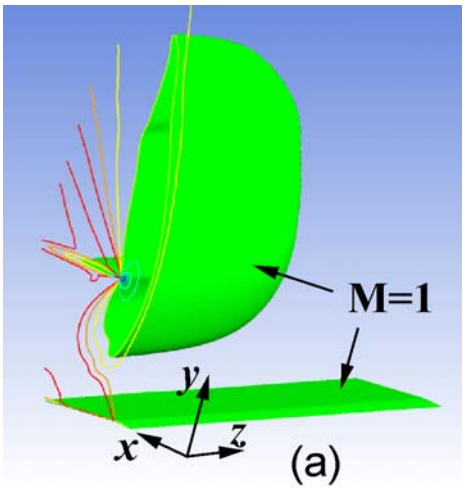

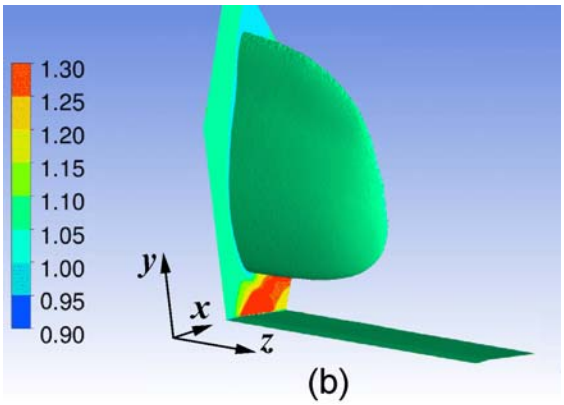

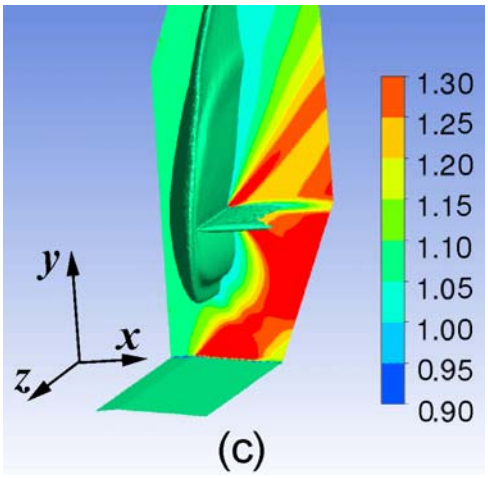

Figure-6. Surfaces M(x,y,z)=1 in 3D flow and Mach number contours in the plane z=0 at M_∞=1.1, L=5/3, θ=8°: (a), (b), (c) – views from three different perspectives

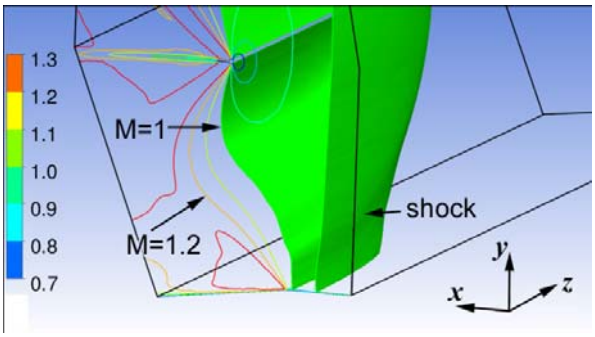

Figure-7. 3D shock wave, the sonic surface M(x,y,z)=1 emanated from the cylinder, and Mach number contours in the plane z=0 at M_∞=1.056, L=5/3, θ=8°. Sonic surfaces in the boundary layers are not visualized for simplicity.

ACKNOWLEDGEMENTS

This research was performed using computational resources provided by the Computational Center of St. Petersburg State University (http://cc.spbu.ru).

REFERENCES

[1] Jameson A. 1991. Airfoils admitting non-unique solutions of the Euler equations. AIAA Paper, No. 91-1625, 1-14.

[2] Hafez M., Guo W. 1999. Nonuniqueness of transonic flows. Acta Mechanica. 138: 177-184.

[3] Kuzmin A. 2013. Instability of transonic flow past flattened airfoils. Central European J. of Engng. 3: 771-775.

[4] Ou K., Jameson A., Vassberg J.C. 2014. Studies of wings supporting non-unique solutions in transonic flows. AIAA Paper. No. 2014-2928, 1-12.

[5] Kuzmin A. 2015. Shock wave instability in a channel with an expansion corner. Int. J. Appl. Mechanics. 7: article 1550019, 1-9.

[6] Kuzmin A. 2016. Shock wave bifurcation in channels with a bend. Archive of Applied Mechanics. 86: 787-795.

[7] Kuzmin A. 2016. Shock wave bifurcation in convergent-divergent channels of rectangular cross section. Shock Waves. 26: DOI: http://link.springer.com/article/10.1007/s00193-016-0624-5.

[8] Zha G-Ch., Knight D., Smith D. 1998. Numerical investigations of HSCT inlet unstart transient at angle of attack. AIAA Paper, No. 98-3583, 1-12.

[9] Hong W., Kim C. 2014. Computational study on hysteretic inlet buzzes characteristics under varying mass flow conditions. AIAA Journal. 52: 1357-1373.

[10] Kuzmin A. 2015. Instability of the shock wave/sonic line interaction. E-print. Centre pour la Communication Scientifique Directe. Centre National de la Recherche Scientifique. France. 1-11. https://hal.archives-ouvertes.fr/hal-01136894/.

[11] Blazek J. 2001. Computational Fluid Dynamics: Principles and Applications. Elsevier. 440 p.

[12] Barth T.J., Jespersen D.C. 1989. The design and application of upwind schemes on unstructured meshes. AIAA Paper. No. 89-0366: 1-12.

[13] Menter F.R. 2009. Review of the Shear-Stress Transport turbulence model experience from an industrial perspective. Int. J. Comput. Fluid Dynamics. 23: 305-316.

[14] Kuzmin A. 2014. On the lambda-shock formation on ONERA M6 wing. Int. J. Applied Engineering Research. 9: 7029-7038.

[15] Kim C.S. 1956. Experimental studies of supersonic flow past a circular cylinder. J. of the Physical Society of Japan. 11: 439-445.

[16] Holder D.W., Chinneck A. 1954. The flow past elliptic-nosed cylinders and bodies of revolution in supersonic air streams. Aeronautical Quarterly. 4: 317-340.

[17] Bashkin V.A., Vaganov A.V., Egorov I.V., Ivanov D.V., Ignatova G.A. 2002. Comparison of calculated and experimental data on supersonic flow past a circular cylinder. Fluid Dynamics. 37: 473-483.